Proceedings of the Twenty-first (2011) International Offshore and Polar Engineering Conference
Maui, Hawaii, USA, June 19-24, 2011

ISBN 978-1-880653-96-8 (Set); ISSN 1098-6189 (Set); www.isope.org

Numerical Simulation of Wave Run-up around a Vertical Cylinder

Hongjian Cao, Jingjing Zha and Decheng Wan
State Key Laboratory of Ocean Engineering, School of Naval Architecture, Ocean and Civil Engineering, Shanghai Jiao Tong University
Shanghai, China

ABSTRACT

Wave run-up and wave impact cause unexpected damage to the offshore platforms. To design a platform against wave impact one must accurately estimate the wave scattering around large volume structures and the maximum run-up height. In this study, simulations of the wave run-up around a fixed vertical cylinder are conducted. The finite volume method (FVM) is employed for solving Navier-Stokes equations based on the open source codes of OpenFOAM. The wave elevations within a radial distance around the cylinder are monitored at several locations. The maximum run-up height is measured, and also the flow field is investigated including the velocity and pressure distributions. The obtained results of wave run-up and scattering around the cylinder are compared with published experiment data. The results show the efficiency of the present numerical method for simulating wave run-up problems, and also provide useful guidance for designing platforms.

KEY WORDS: Wave run-up; cylinder; numerical wave tank; OpenFOAM.

INTRODUCTION

Wave run-up and wave impact can cause unexpected damage to offshore structures. Therefore, the design of offshore structures requires accurate predictions of the maximum wave elevation to maintain sufficient airgap below the platform deck. Accurate prediction of wave run-up can both help reducing building costs and avoid the risk of wave impact and damage to the platform. For the increasing number of offshore platforms built for ocean oil and gas exploration, the investigation of wave run-up becomes more and more significant for the design of fixed offshore structures.

Wave run-up on circular cylinders has been studied experimentally and numerically in the past decades. Niedzwecki & Duggal (1992) performed a small-scale experiment to study the wave run-up on a truncated circular cylinder. Martin *et al.* (2001) investigated run-up on columns caused by steep, deep water regular waves and concluded that linear diffraction theory was inadequate. Experiment investigations were also carried out by Mase *et al.* (2001) and De Vos *et al.* (2007), and empirical formulas were given to predict the wave run-up. Based on the experiments performed by MARINTEK (Nielsen, 2003) and Morris-Thomas & Thiagarajan (2004), a series of experimental data was published. The model test performed at MARINTEK was proposed as the ISSC benchmark study. The wave run-up results obtained by different numerical methods were proposed and compared with the MARINTEK data.

In previous works the focus has been the horizontal forces, whereas the wave run-up has been studied in less detail. With the linear diffraction theory, the approximate run-up ratio function was given, e.g. in MacCamy & Fuchs (1954) and Haney & Herbich (1982). Linear diffraction theory predicted that run-up height is a function of the scattering parameter $\boldsymbol{ka}$, where $\boldsymbol{k}$ is the wave number and $\boldsymbol{a}$ is the cylinder radius. Kriebel (1990, 1992) presented the solution of the nonlinear wave–cylinder interaction and predicted that the solution of linear diffraction theory was under-predicted for run-up in larger waves.
With the development of numerical techniques, time domain simulations became to an alternative for wave run-up and wave-structure interaction problem. Buchmann *et al.* (1998) used a second-order boundary element model for the wave run-up problem. Trulsen & Teigen (2002) applied the fully nonlinear potential method for computing the wave scattering around a vertical cylinder. Lee *et al.* (2007) simulated the wave run-up on vertical cylinder by a 3-diensional VOF method based on a two-step projection, and discussed the nonlinear wave-cylinder interaction. Danmeier *et al.* (2008) compared the wave run-up results from a second-order diffraction code (WAMIT) and a fully nonlinear CFD program (ComFLOW) with the experiments.

In recent years, lots of commercial CFD software has been employed for solving the wave-structure interaction problem such as Fluent, CFX, Flow-3D, etc. However, for commercial interests, the source codes of these commercial packages are not opened to the user, which has restricted the development of CFD methods. The Open source Field Operation and Manipulation (OpenFOAM) C++ libraries provide users the open source codes for developing new CFD methods. The user can not only use OpenFOAM as software, but also can modify all the codes of OpenFOAM, even create new solvers and numerical schemes for particular problems. The object-oriented C++ programming language lays a good basis for the development of OpenFOAM, as well as the development of CFD.

In the present study, simulations of wave run-up on a fixed cylinder are conducted by employing the Finite Volume Method (FVM) to solve the Navier-Stokes equations based on the open source codes of OpenFOAM.

The Volume of Fluid (VOF) technique is used to capture the water-air interface. For generating the incident waves, a 3-dimensional numerical wave tank with piston-type wave-maker is constructed using the moving-mesh technique.

This paper is organized as follow: First, the numerical method is introduced. Then, the computational model configurations of numerical wave tank are described. The incident waves are generated and a grid convergence test is carried out. The cases of wave run-up on fixed cylinder are simulated and the results are presented and discussed. Furthermore, the dynamic pressure and velocity near the cylinder are presented. Finally, a brief conclusion is drawn.

NUMERICAL METHOD

Governing Equations

In the present study, both the air and water phases are considered incompressible. The governing equations for the incompressible, viscous fluid flow include the continuity equation and the Navier-Stokes equations as follows：

Continuity equation

$$\nabla \cdot \vec{u} = 0 \tag{1}$$

Navier-Stokes equations

$$\frac{\partial(\rho\vec{u})}{\partial t} + \nabla(\rho\vec{u}\vec{u}) = -\nabla p + \nabla\cdot(\mu\nabla\vec{u}) + \rho\vec{g} + \vec{F}_s \tag{2}$$

where $\vec{u}$, *p*, *ρ*, *ν* and g denote the velocity， pressure, density, kinematics viscosity and acceleration of gravity respectively. $\vec{F}_s$ is the free surface tension and it takes place only at the water-air interface. It can be expressed as

$$\vec{F}_s = \sigma\kappa(x)\vec{n} \ , \tag{3}$$

where $\vec{n}$ and κ are the unit normal vector and curvature of the interface, and σ is a constant. Here κ is given by

$$\kappa(x) = \nabla\cdot\vec{n} \ . \tag{4}$$

The VOF technique is used for capture the water-air interface which is determined by solving the volume fraction function. The following equation is used:

$$\frac{\partial\gamma}{\partial t} + \nabla\cdot(\gamma\vec{u}) = 0 \tag{5}$$

Here γ denotes the volume fraction of one fluid in a cell. Thus, we have $0 \le \gamma \le 1$, and the iso-contour of $\gamma = 0.5$ is considered as the interface.

In the computation, 3-dimensional body fitted mesh is generated in the computational domain and the FVM is applied to discretize the governing equations based on the codes of interDymFoam solver in OpenFOAM. The PISO algorithm is used during the computation.

Numerical Wave Tank

Wave generation and wave absorbing are two important parts of the numerical wave tank. In the present study, incident waves are generated by a piston-type wave-maker located at the left end of the rectangular wave tank, and propagating in the positive *x*-direction.

According to the linear wave maker theory (Usell *et al.*, 1960), for the generation of a wave with a surface elevation

$$\zeta = \frac{H}{2}\cos(kx - \omega t) \tag{6}$$

where k is the wave-number, and ω is the angular frequency, the displacement of the piston is determined as:

$$x(t) = \frac{S}{2}\sin\omega t \ . \tag{7}$$

Here, *S* denotes the stroke of the piston, and is given by

$$S = H\left(\frac{2kd + \sinh(2kd)}{4\sinh^2(kd)}\right) \tag{8}$$

The piston's motion is implemented by employing a moving-mesh technique. The topology of the mesh does not change while the piston is moving, but only the spacing between (almost all) nodes changes by stretching and squeezing. The positions of the mesh points in the field are determined by solving a Laplace equation with constant or variable diffusivity. In the presented cases, the diffusivity is based linearly on the inverse of the cell center distance to the piston boundary.

For wave absorbing, a wave damping zone, also called sponge layer (Larsen & Dancy, 1983), is set to avoid the wave reflection at the end of the tank. The damping coefficient ν is nonzero within the damping zone $[x_0, x_1]$, and given by:

$$\nu(x) = \begin{cases} \alpha(x - x_0)/(x_1 - x_0), & x \in [x_0, x_1] \\ 0, & ortherwise \end{cases} \tag{9}$$

Here, α is a dimensionless parameter adjusted depending on the wave damping effect.

NUMERICAL SIMULATION AND RESULTS

Model Test Configurations

The wave run-up around the vertical cylinder was investigated experimentally at MARINTEK. This case has been used as an ISSC benchmark study (Nielsen, 2003) with the full scale model. In the present study, a similar full scale test is set up for the simulations.

The diameter of the circular cylinder is *D*=16.0m, and the draft of the cylinder is 24.0m. The wave elevation is measured at 12 locations in the vicinity of the cylinder. The locations of the probes are given in Table 1. The radial distance is measured from the center of the cylinder. The positions are illustrated in Fig. 1.

Table 1. Positions where the wave elevation is measured

Row	Direction (deg)	Radial distances (m)point no. 1, 2, 3 and 4
A1	270	8.05, 9.47, 12.75, 16.0
A2	225	8.05, 9.47, 12.75, 16.0
A3	180	8.05, 9.47, 12.75, 16.0

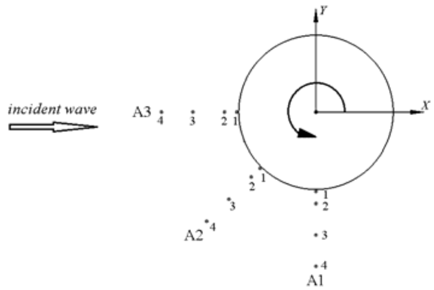

Fig. 1. Positions where the wave elevation is measured

In the present simulations, the incident wave conditions are limited to regular waves. The parameters of the waves are shown in Table 2. The wave is assumed to be deep-water wave so that the wave length λ=126.5m can be obtained with the wave period T=9s. In the following part of this paper, wave M1 stands for the wave with wave height H=4.22m and wave M2 for H=7.99m.

Table 2. Parameters of incident wave conditions

Wave	Height H (m)	Period T (s)	Steepness H/λ
M1	4.22	9	1/30
M2	7.99	9	1/16

The length of the numerical wave tank is set as L=10λ, and the width B=320m. The total height of the wave tank is 224m including 24m air part and 200m water depth. At the right end of the tank, a 2λ length wave damping zone is used. The numerical wave tank is shown as Fig. 2. The circular cylinder is located in the middle part of the tank with a distance about 4λ from the piston as shown in Fig. 3, and the draft of the cylinder is 24m at initial time.

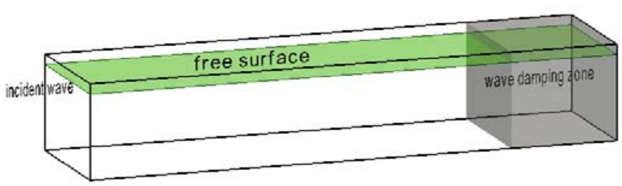

Fig. 2. Computational model of numerical wave tank

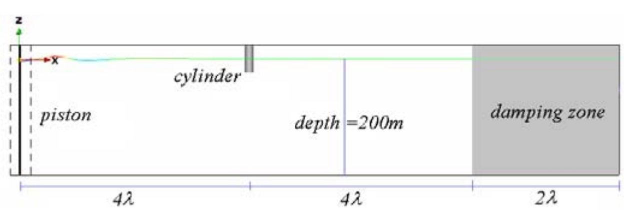

Fig. 3. Configurations of wave run-up case

Cylinder Surface and outlet boundary are non-slip wall condition. The bottom of tank is slip wall condition. To avoid the influence of the boundaries to the flow field, symmetry boundary condition is applied to both sides of the tank. The piston boundary is also non-ship wall but with motion. The displacement of the piston is defined and updated at each time step according to Eq. 7.

Incident Wave Generation

First of all, the incident waves must be generated accurately in order to obtain successful wave run-up simulations. Thus, without the cylinder in the numerical wave tank, the incident waves are generated and the wave elevation at the position of the cylinder center is measured to check the accuracy of the wave generation method.

To validate the mesh convergence of the computation, three different meshes are used for simulating the wave M1 (H=4.22m). The details of the meshes are shown in Table 3.

Table 3. The grid convergence test for the wave generation

Mesh	Total Cell Count	$\lambda/\Delta x$	$H/\Delta z_{\min}$
I	769216	21	8
II	835312	23	10
III	879648	25	12

Fig. 4 shows the comparison of the time histories of the wave elevation at the position of the cylinder center with the three different meshes. Good agreement can be achieved but a small difference is found at the wave crest and trough. The wave crest height is almost the same with the incident wave height, whereas the wave trough becomes flat due to the nonlinear effects.

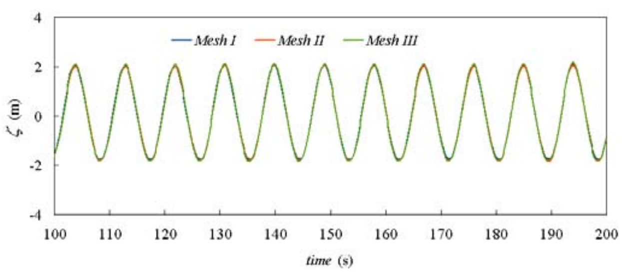

Fig. 4. Time history of the incident wave M1 at the location of the cylinder center

With the finest mesh, the wave damping along the wave tank is very small, the obtained mean crest heights of wave M1 and wave M2 are about 2.0m and 3.8m. The difference between the target and obtained wave crest value is very small, and below 6%. Fig. 5 shows the time history of the incident wave M2 at the location of the cylinder center.

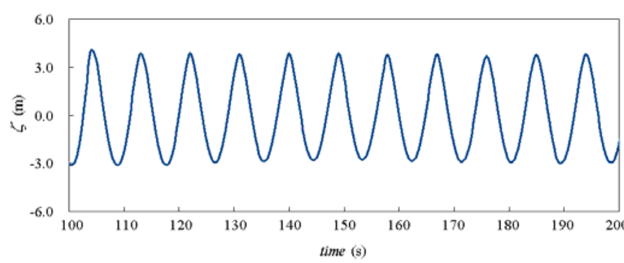

Fig. 5. Time history of the incident wave M2 at the location of the cylinder center

The simulated wave surface along the wave tank is illustrated in Fig. 6.

The wave elevation is gradually decreased to be zero at the end of wave tank, which shows the efficiency of the wave damping zone.

To ensure the accuracy of incident wave condition, the finest grids is used for the following wave run-up cases.

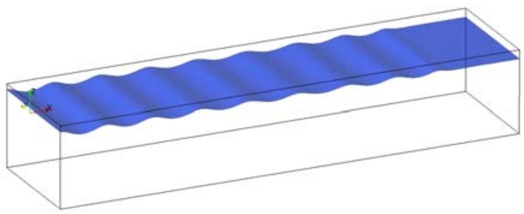

Fig. 6. Free surface along the wave tank, for wave M1

Wave Run-up Simulation

In this section, wave run-up around the vertical circular cylinder is simulated, and the results are presented and analyzed.

First, by comparing the horizontal wave force, the mesh convergence is also validated with three different meshes. Only structured hexahedral meshes are generated for the simulation. The global mesh and detail local mesh near the cylinder are shown in Fig.7. The details of the mesh are shown in Table 4. The only difference is the grid count along the cylinder circle.

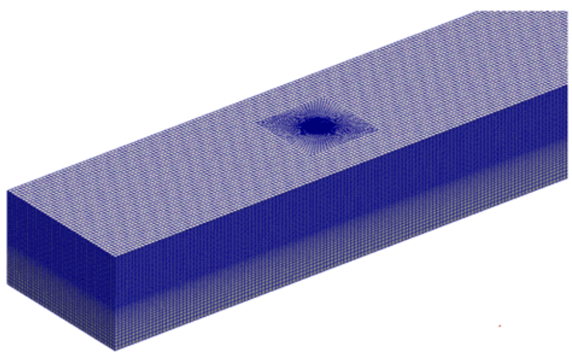

(a)

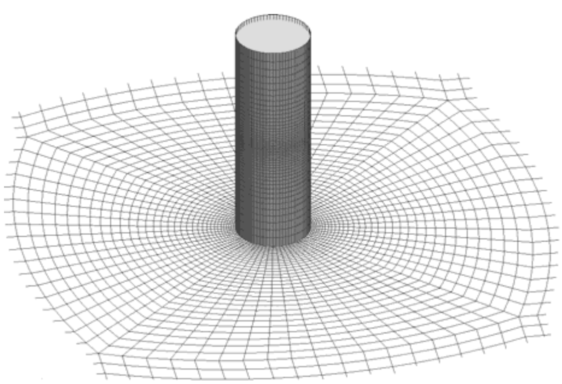

(b)

Fig. 7. Computational mesh: (a) Global mesh, (b) Local detail mesh near the cylinder.

Table 4. The details of the grids for the grid convergence test.

Mesh	Total cell count	Grid count along the circle
I	790960	56
II	830496	64
III	881568	72

With the incident wave M1, we simulated the wave run-up case with the above three meshes, and calculated the horizontal forces on the cylinder. Fig. 8 shows the horizontal forces, from which the convergence can be seen while the cell count is over 0.8 million.

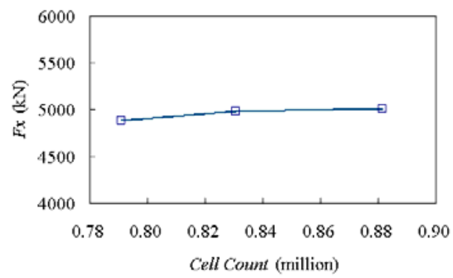

Fig. 8. Horizontal force *Fx* on the cylinder, for wave M1

Thus, all the wave run-up cases are simulated with the finest grid, and the results are presented in the following section.

Numerical Results

Wave forces on the cylinder

The wave forces on the cylinder are calculated for both wave M1 and wave M2. For wave M1, the obtained horizontal force *Fx* is about 5000kN, and the vertical force *Fz* is about 1000kN. The time histories of *Fx* and *Fz* are shown as Fig. 9. For wave M2, the obtained horizontal force *Fx* is about 9000kN, and the vertical force *Fz* is about 1800kN. The time histories of *Fx* and *Fz* are shown as Fig. 10.

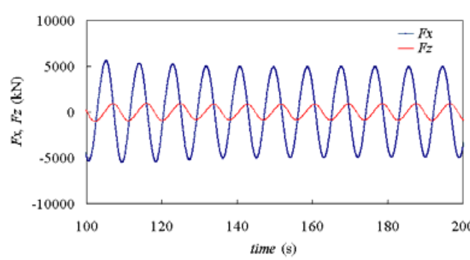

Fig. 9. Time history of *Fx* and *Fz* on the cylinder, for wave M1

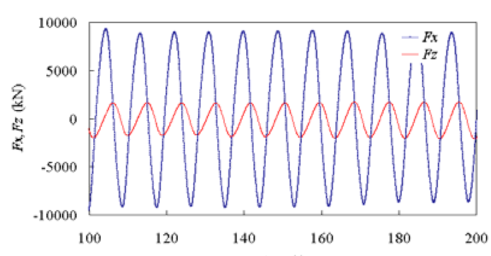

Fig. 10. Time history of *Fx* and *Fz* on the cylinder, for wave M2

Free surface

The free surface elevations are measured at probes along A1, A2 and A3. Fig. 11 and Fig. 12 show the time series at probes along line A1 (270 degree) for wave M1 and wave M2.

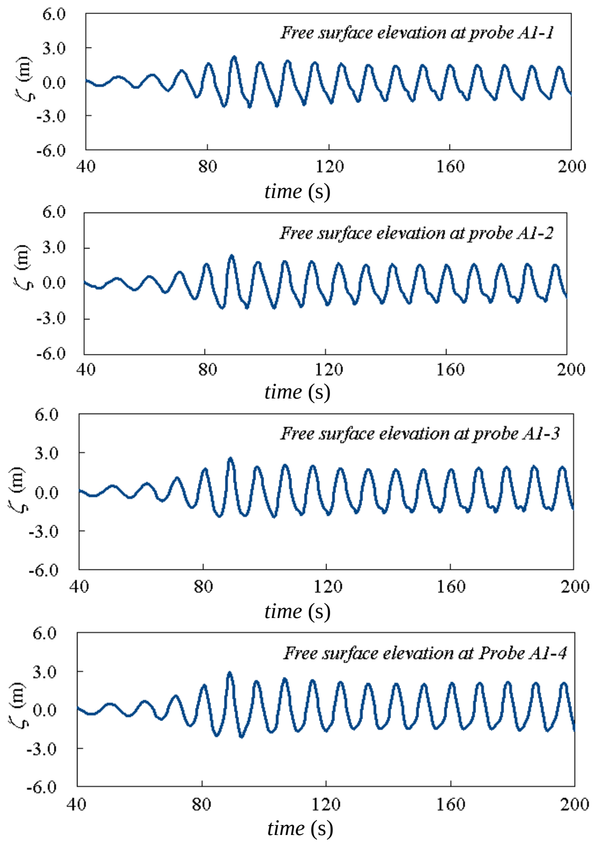

Fig. 11. Free surface elevation at probes along row A1, for wave M1

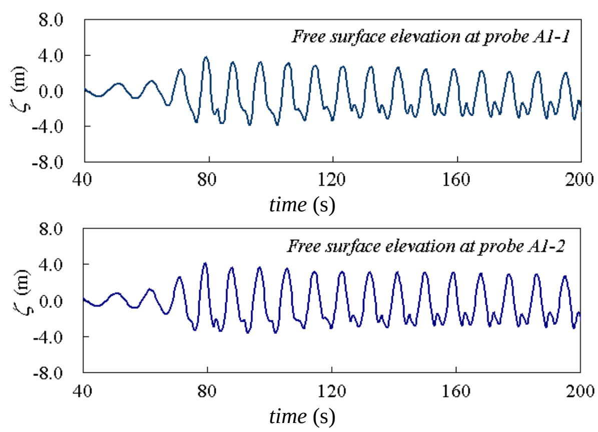

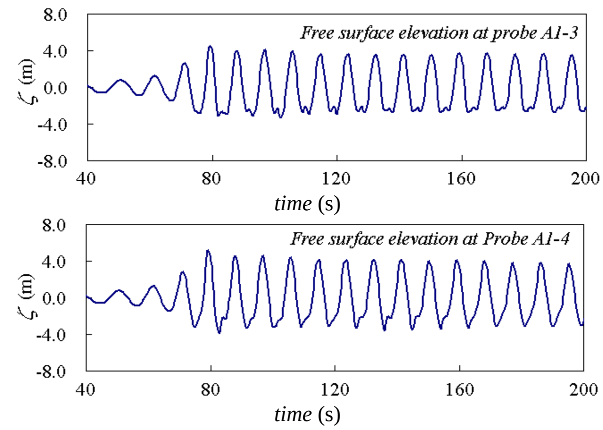

Fig. 12. Free surface elevation at probes along row A1, for wave M2

With increasing heights of incident waves, the nonlinear wave effect on the cylinder becomes stronger, while the wave run-up becomes higher. Comparing time series of free surface elevations at probes along row A1 for wave M1 and M2, we can see that the wave elevations change much violently at the trough in a wave period for incident wave M2. There is a secondary crest appearing at the trough in a wave period for wave M2. This phenomenon was also observed in the experiments (Morris-Thomas, 2003).

From the free surface elevation contours shown in Fig. 13 and Fig. 14, strong wave impact on cylinder can be seen, especially for wave M2

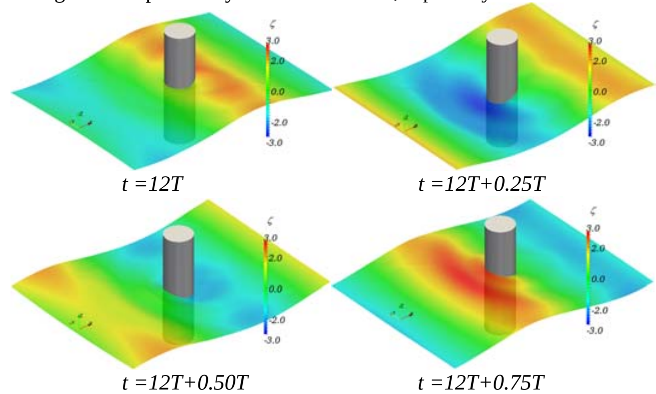

Fig. 13. Free surface elevation, for wave M1

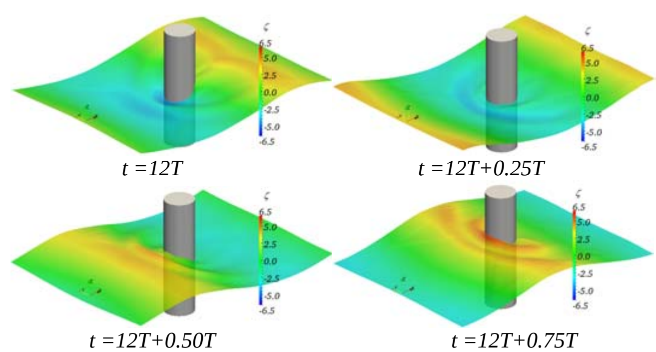

Fig. 14. Free surface elevation, for wave M2

The maximum wave run-up in front of the cylinder often happened close to the cylinder surface. As showed in Fig. 15 and Fig. 16, the wave elevation near the cylinder along the longitudinal section of the tank in a wave period is illustrated, from which the phenomenon of wave run-up can be seen clearly and the maximum wave run-up height is obtained at about *t=115s*. The velocity and pressure contours of the free surface at *t=12.75T* for wave M1 and M2 are shown in Fig. 17.

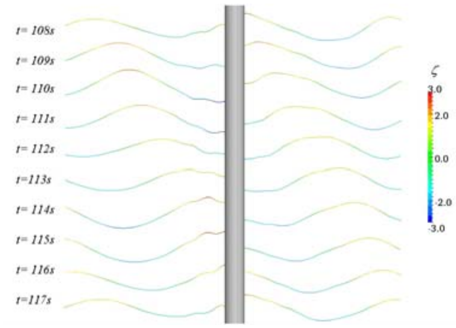

Fig. 15. Free surface elevation form *12T to 13T*, for wave M1

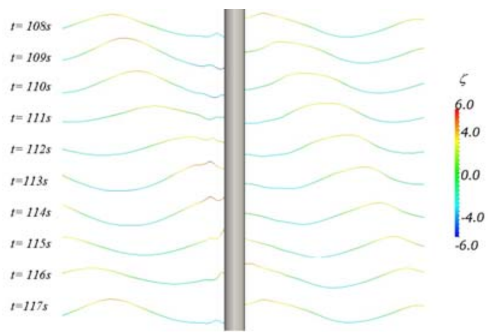

Fig. 16. Free surface elevation form *12T to 13T*, for wave M2

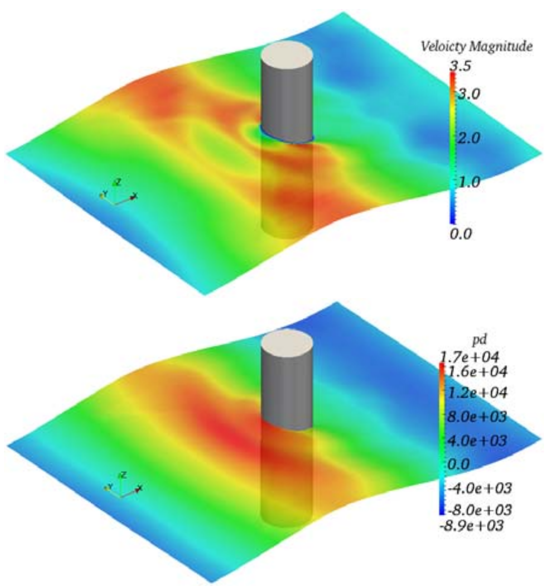

(a) wave M1

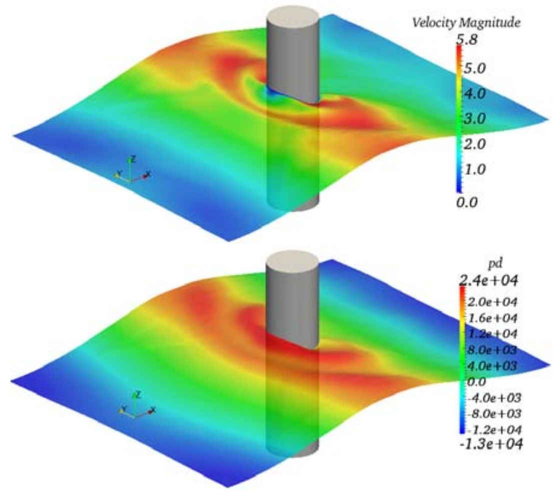

(b) wave M2

Fig. 17. Velocity and pressure contour of the free surface at *t=12.75T*: (a) wave M1, (b) Wave M2.

Since the viscous flow effect is considered in the simulations, the vortex shedding due to the presence of the cylinder can be attained. In Fig. 18, the contours of vorticity component ω_x close to the free surface for M1 are illustrated, which reflect that there are vortexes appearing and shedding from the cylinder surface. Therefore, the vortex shedding also has important influence to the wave run-up value.

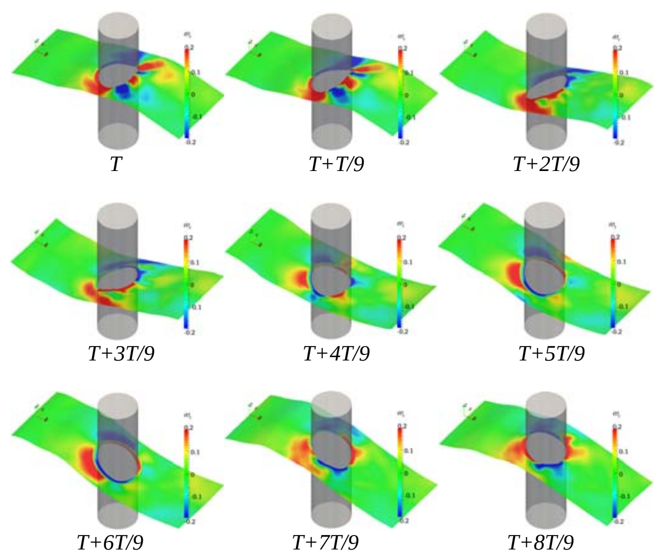

Fig. 18. Vorticity component ω_x contour of the free surface in a period *T*, for wave M1

Wave run-up ratio comparison

Now we focus on the wave run-up heights at fixed probes along row A1, A2 and A3. The obtained simulated results are compared with the experimental data.

In order to attain the average maximum crest elevation, about 12 wave periods starting at about 80s in the time series of the free surface elevation are used to perform the analysis.

The comparisons between the simulation and the experimental wave run-up data are shown in Fig. 19 and Fig. 20. ***ζ*** *is* the average maximum crest elevation; ***A*** is the crest height of incident wave, given by ***A***= *H/2* ; ***r*** is the radial distance from the cylinder center and ***a*** is the radius of the cylinder. We can see that the present maximum wave run-up ratio agrees well with the experimental data. The maximum crest elevation is measured at the first probe along row A3, the nearest probe in front of the cylinder. The maximum value of wave run-up ratio is about 1.4 with the incident wave M1, and 1.6 with the incident wave M2.

However, the largest difference between simulation and experimental data happens at the second probe in row A3 (180 degree), especially for wave M2. The maximum crest value happens at the probe A3-2 according to experimental data, whereas at the A3-1 according to the simulation. The present maximum crest elevation decreases very fast from A3-1 to A3-2. A similar difference also appears in most numerical results from boundary element methods (BEM) presented in Nielsen (2003). This may be due to the interaction of oncoming wave and the wave reflected back from the cylinder.

For the other probes, the maximum crest value is a bit under-predicted if compared with the experimental data. Note that the present incident waves are generated based on the linear wave theory, it may have great influence to the wave run-up height. Thus, more work will be continued on the wave run-up problem with higher order incident waves.

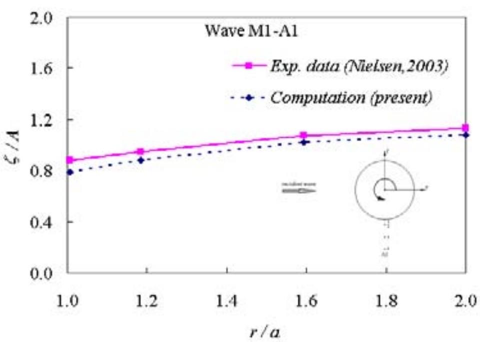

(a)

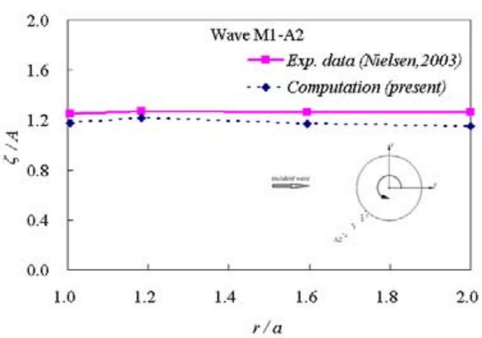

(b)

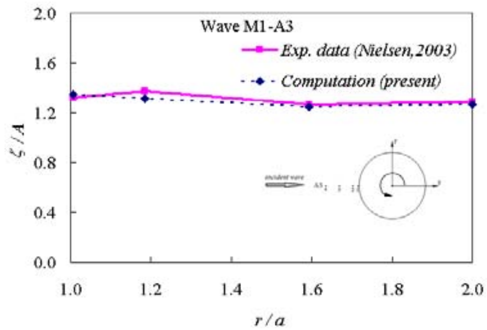

(c)

Fig. 19. Maximum wave run-up elevation at probes along: (a) row A1, (b) row A2, (c) row A3; for wave M1

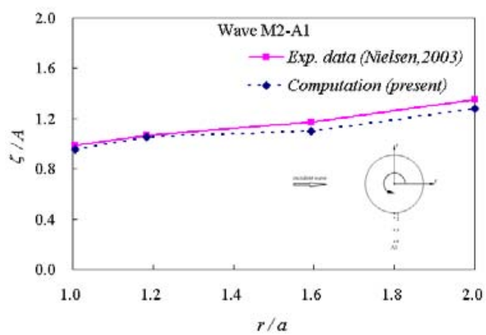

(a)

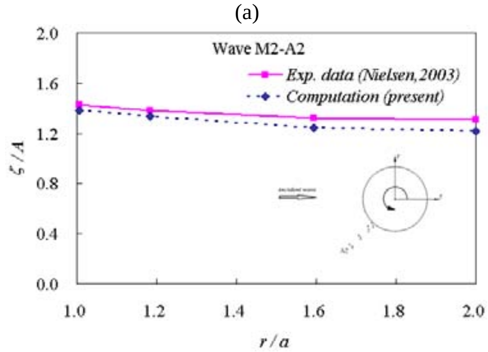

(b)

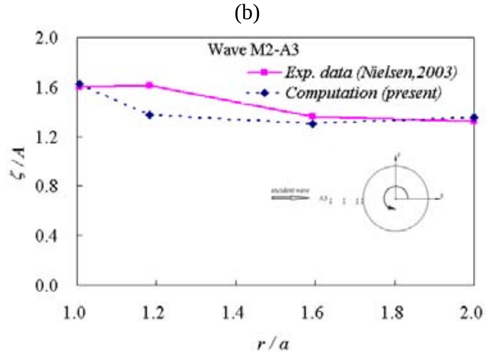

(c)

Fig. 20. Maximum wave run-up elevation at probes along: (a) row A1, (b) row A2, (c) row A3; for wave M2

CONCLUSIONS

The simulations of wave run-up around a vertical cylinder by means of the CFD codes provided by OpenFOAM have been presented. The numerical results agree well with the experimental data. However, some difference of the wave run-up is found at some of the probes.

From these results, it is found that the wave run-up on fixed cylinder problem is simulated well, and the obtained wave run-up height is reasonable. The information of flow field obtained can provide the useful guidance for the design of platforms. Since the time consuming would be very large as the mesh number increases, the simulations presented are not at the best accuracy. Meanwhile, the use of a higher order incident wave may help to obtain better results. Furthermore, the waves reflected by the cylinder back to wave-maker may influence the incident wave. Thus, only several wave periods' data can be used for analysis.

The presented results show the good efficiency of the numerical method for simulating the wave run-up problem. Based on the codes of OpenFOAM, more work can be solved such as simulating the 6-DOF movement of the floating platform in wave and current. Obviously, with the suitable and efficient CFD tool OpenFOAM, lots of ocean engineering problems can be solved and more contributions to the design of the offshore structures. can be achieved.

ACKNOWLEDGEMENTS

The support of National Natural Science Foundation of China (Grant No. 11072154, 50739004), Research Foundation of State Key Laboratory of Ocean Engineering of China (Grant No. GKZD010064) and the Program for Professor of Special Appointment (Eastern Scholar) at Shanghai Institutions of Higher Learning for this work is gratefully acknowledged.

REFERENCES

Buchmann, B, Skourup, J, and Cheung, Kwok Fai (1998). "Run-up on a structure due to second-order waves and a current in a numerical wave tank," *Applied Ocean Research*, Vol 20, pp 297-308.

De Vos, L, Frigaard, P and De Rouck, J (2007). "Wave run-up on cylindrical and cone shaped foundations for offshore wind turbines," *Coastal Eng*, Vol 54, pp 17-29.

Danmeier, DG, Seah, RKM, Finnigan, T, Roddier, D, Aubault A, Vache, M and Imamura JT (2008). "Validation of wave run-up calculation methods for a gravity based structure," *Proc ASME 27th Int Conf Offshore Mech. and Arct Eng,* Estoril, Portugal, paper No: OMAE2008-57625

Haney, JP and Herbich, JB (1982). "Wave flow around thin piles and piles groups," *J Hydraul Res*, Vol. 20, No. 1, pp 1-14.

Kriebel, DL (1990). "Nonlinear wave interaction with a vertical circular cylinder. Part I: diffraction theory," *Ocean Eng*, Vol 17, No 4, pp 345-377.

Kriebel, DL (1992). "Nonlinear wave interaction with a vertical circular cylinder. Part II: Wave run-up," *Ocean Eng*, Vol 19, No 1, pp 75-99.

Larsen, Jesper, and Dancy Henry (1983). "Open boundaries in short wave simulations - a new approach," *Coastal Eng*, Vol 7, pp 285-297.

Lee, KH, Kim, DS, Kim, CH, Lee, SK, and Kee, ST (2007). "Wave run-up on vertical cylinder by 3-dimensional VOF method," *Proc 17th Int Offshore and Polar Eng Conf,* Lisbon, Portugal, ISOPE, pp 2679-2683.

MacCamy, RC and Fuchs, RA (1954). "Wave force on piles: A diffraction theory." *Beach Erosion Board Office of the Chief Engineers, Department of the Army, Technical Memo* No. 69, pp 1–17.

Martin, AJ, Easson, WJ, and Bruce, T (2001). "Run-up on columns in steep, deep water regular waves," *J Waterway, Port, Coastal, and Ocean Eng*, Vol 127, No 1, pp 26-32.

Mase, H, Kosho, K, and Nagahashi, S (2001). "Wave run-up of random waves on a small circular pier on sloping seabed," *J Waterway, Port, Coastal, and Ocean Eng*, Vol 127, No 4, pp 192-199.

Morris-Thomas, MT (2003). "Wave run up on vertical columns of an offshore structure," *The University of Western Australia*, PhD Thesis.

Morris-Thomas, MT and Thiagarajan, KP (2004). "The run-up on a cylinder in progressive surface gravity waves: harmonic components," *Appl Ocean Res*, Vol 24, pp 98-113.

Niedzwecki, JM and Duggal, SD (1992). "Wave run-up and forces on cylinders in regular and random waves," *J Waterway, Port, Coastal, and Ocean Eng*, Vol 118, No 6, pp 615-634.

Nielsen, FG (2003). "Comparative study on airgap under floating platforms and run-up along platform columns," *Marine Structures*, Vol 16, pp 97-134.

Trulsen, Karsten and Teigen, Per (2002). "Wave scattering around a vertical cylinder: fully nonlinear potential flow calculations compared with low order perturbation results and experiment," *Proc 21st Int Conf Offshore Mech and Artic Eng,* Oslo, Norway. paper No:OMAE2002-28173.

Ursell, F, Dean, RG, and Yu YS (1960). "Forced small-amplitude waters: a comparison of theory and experiment," *J. Fluid Mech*, Vol 7, pp 32-53.